EUROPEAN ORGANIZATION FOR NUCLEAR RESEARCH

CERN-EP-2001-066
20 September 2001

Search for Single Top Quark Production at LEP2

The OPAL Collaboration

Abstract

A search for single top quark production via flavour changing neutral currents (FCNC) was performed with data collected by the OPAL detector at the e^+e^- collider LEP. Approximately 600 pb^{-1} of data collected at $\sqrt{s} = 189$ - $209\,GeV$ were used to search for the FCNC process $e^+e^- \to tc(u) \to bWc(u)$. This analysis is sensitive to the leptonic and the hadronic decay modes of the W boson. No evidence for a FCNC process is observed. Upper limits at the 95% confidence level on the single top production cross-section as a function of the centre-of-mass energy are derived. Limits on the anomalous coupling parameters κ_γ and κ_Z are determined from these results.

(Submitted to Physics Letters B)

The OPAL Collaboration

G. Abbiendi[2], C. Ainsley[5], P.F. Åkesson[3], G. Alexander[22], J. Allison[16], G. Anagnostou[1], K.J. Anderson[9], S. Arcelli[17], S. Asai[23], D. Axen[27], G. Azuelos[18,a], I. Bailey[26], E. Barberio[8], R.J. Barlow[16], R.J. Batley[5], T. Behnke[25], K.W. Bell[20], P.J. Bell[1], G. Bella[22], A. Bellerive[6], G. Benelli[4], S. Bethke[32], O. Biebel[32], I.J. Bloodworth[1], O. Boeriu[10], P. Bock[11], J. Böhme[25], D. Bonacorsi[2], M. Boutemeur[31], S. Braibant[8], L. Brigliadori[2], R.M. Brown[20], H.J. Burckhart[8], J. Cammin[3], R.K. Carnegie[6], B. Caron[28], A.A. Carter[13], J.R. Carter[5], C.Y. Chang[17], D.G. Charlton[1,b], P.E.L. Clarke[15], E. Clay[15], I. Cohen[22], J. Couchman[15], A. Csilling[8,i], M. Cuffiani[2], S. Dado[21], G.M. Dallavalle[2], S. Dallison[16], A. De Roeck[8], E.A. De Wolf[8], P. Dervan[15], K. Desch[25], B. Dienes[30], M.S. Dixit[6,a], M. Donkers[6], J. Dubbert[31], E. Duchovni[24], G. Duckeck[31], I.P. Duerdoth[16], E. Etzion[22], F. Fabbri[2], L. Feld[10], P. Ferrari[12], F. Fiedler[8], I. Fleck[10], M. Ford[5], A. Frey[8], A. Fürtjes[8], D.I. Futyan[16], P. Gagnon[12], J.W. Gary[4], G. Gaycken[25], C. Geich-Gimbel[3], G. Giacomelli[2], P. Giacomelli[2], D. Glenzinski[9], J. Goldberg[21], K. Graham[26], E. Gross[24], J. Grunhaus[22], M. Gruwé[8], P.O. Günther[3], A. Gupta[9], C. Hajdu[29], M. Hamann[25], G.G. Hanson[12], K. Harder[25], A. Harel[21], M. Harin-Dirac[4], M. Hauschild[8], J. Hauschildt[25], C.M. Hawkes[1], R. Hawkings[8], R.J. Hemingway[6], C. Hensel[25], G. Herten[10], R.D. Heuer[25], J.C. Hill[5], K. Hoffman[9], R.J. Homer[1], D. Horváth[29,c], K.R. Hossain[28], R. Howard[27], P. Hüntemeyer[25], P. Igo-Kemenes[11], K. Ishii[23], A. Jawahery[17], H. Jeremie[18], C.R. Jones[5], P. Jovanovic[1], T.R. Junk[6], N. Kanaya[26], J. Kanzaki[23], G. Karapetian[18], D. Karlen[6], V. Kartvelishvili[16], K. Kawagoe[23], T. Kawamoto[23], R.K. Keeler[26], R.G. Kellogg[17], B.W. Kennedy[20], D.H. Kim[19], K. Klein[11], A. Klier[24], S. Kluth[32], T. Kobayashi[23], M. Kobel[3], T.P. Kokott[3], S. Komamiya[23], R.V. Kowalewski[26], T. Krämer[25], T. Kress[4], P. Krieger[6], J. von Krogh[11], D. Krop[12], T. Kuhl[3], M. Kupper[24], P. Kyberd[13], G.D. Lafferty[16], H. Landsman[21], D. Lanske[14], I. Lawson[26], J.G. Layter[4], A. Leins[31], D. Lellouch[24], J. Letts[12], L. Levinson[24], J. Lillich[10], C. Littlewood[5], S.L. Lloyd[13], F.K. Loebinger[16], G.D. Long[26], M.J. Losty[6,a], J. Lu[27], J. Ludwig[10], A. Macchiolo[18], A. Macpherson[28,l], W. Mader[3], S. Marcellini[2], T.E. Marchant[16], A.J. Martin[13], J.P. Martin[18], G. Martinez[17], G. Masetti[2], T. Mashimo[23], P. Mättig[24], W.J. McDonald[28], J. McKenna[27], T.J. McMahon[1], R.A. McPherson[26], F. Meijers[8], P. Mendez-Lorenzo[31], W. Menges[25], F.S. Merritt[9], H. Mes[6,a], A. Michelini[2], S. Mihara[23], G. Mikenberg[24], D.J. Miller[15], S. Moed[21], W. Mohr[10], T. Mori[23], A. Mutter[10], K. Nagai[13], I. Nakamura[23], H.A. Neal[33], R. Nisius[8], S.W. O'Neale[1], A. Oh[8], A. Okpara[11], M.J. Oreglia[9], S. Orito[23], C. Pahl[32], G. Pásztor[8,i], J.R. Pater[16], G.N. Patrick[20], J.E. Pilcher[9], J. Pinfold[28], D.E. Plane[8], B. Poli[2], J. Polok[8], O. Pooth[8], A. Quadt[3], K. Rabbertz[8], C. Rembser[8], P. Renkel[24], H. Rick[4], N. Rodning[28], J.M. Roney[26], S. Rosati[3], K. Roscoe[16], Y. Rozen[21], K. Runge[10], D.R. Rust[12], K. Sachs[6], T. Saeki[23], O. Sahr[31], E.K.G. Sarkisyan[8,m], C. Sbarra[26], A.D. Schaile[31], O. Schaile[31], P. Scharff-Hansen[8], M. Schröder[8], M. Schumacher[25], C. Schwick[8], W.G. Scott[20], R. Seuster[14,g], T.G. Shears[8,j], B.C. Shen[4], C.H. Shepherd-Themistocleous[5], P. Sherwood[15], A. Skuja[17], A.M. Smith[8], G.A. Snow[17], R. Sobie[26], S. Söldner-Rembold[10,e], S. Spagnolo[20], F. Spano[9], M. Sproston[20], A. Stahl[3], K. Stephens[16], D. Strom[19], R. Ströhmer[31], L. Stumpf[26], B. Surrow[25], S. Tarem[21], M. Tasevsky[8], R.J. Taylor[15], R. Teuscher[9], J. Thomas[15], M.A. Thomson[5], E. Torrence[19], D. Toya[23], T. Trefzger[31], A. Tricoli[2], I. Trigger[8], Z. Trócsányi[30,f], E. Tsur[22],

M.F. Turner-Watson[1], I. Ueda[23], B. Ujvári[30,f], B. Vachon[26], C.F. Vollmer[31], P. Vannerem[10], M. Verzocchi[17], H. Voss[8], J. Vossebeld[8], D. Waller[6], C.P. Ward[5], D.R. Ward[5], P.M. Watkins[1], A.T. Watson[1], N.K. Watson[1], P.S. Wells[8], T. Wengler[8], N. Wermes[3], D. Wetterling[11] G.W. Wilson[16], J.A. Wilson[1], T.R. Wyatt[16], S. Yamashita[23], V. Zacek[18], D. Zer-Zion[8,k]

[1]School of Physics and Astronomy, University of Birmingham, Birmingham B15 2TT, UK
[2]Dipartimento di Fisica dell' Università di Bologna and INFN, I-40126 Bologna, Italy
[3]Physikalisches Institut, Universität Bonn, D-53115 Bonn, Germany
[4]Department of Physics, University of California, Riverside CA 92521, USA
[5]Cavendish Laboratory, Cambridge CB3 0HE, UK
[6]Ottawa-Carleton Institute for Physics, Department of Physics, Carleton University, Ottawa, Ontario K1S 5B6, Canada
[8]CERN, European Organisation for Nuclear Research, CH-1211 Geneva 23, Switzerland
[9]Enrico Fermi Institute and Department of Physics, University of Chicago, Chicago IL 60637, USA
[10]Fakultät für Physik, Albert Ludwigs Universität, D-79104 Freiburg, Germany
[11]Physikalisches Institut, Universität Heidelberg, D-69120 Heidelberg, Germany
[12]Indiana University, Department of Physics, Swain Hall West 117, Bloomington IN 47405, USA
[13]Queen Mary and Westfield College, University of London, London E1 4NS, UK
[14]Technische Hochschule Aachen, III Physikalisches Institut, Sommerfeldstrasse 26-28, D-52056 Aachen, Germany
[15]University College London, London WC1E 6BT, UK
[16]Department of Physics, Schuster Laboratory, The University, Manchester M13 9PL, UK
[17]Department of Physics, University of Maryland, College Park, MD 20742, USA
[18]Laboratoire de Physique Nucléaire, Université de Montréal, Montréal, Quebec H3C 3J7, Canada
[19]University of Oregon, Department of Physics, Eugene OR 97403, USA
[20]CLRC Rutherford Appleton Laboratory, Chilton, Didcot, Oxfordshire OX11 0QX, UK
[21]Department of Physics, Technion-Israel Institute of Technology, Haifa 32000, Israel
[22]Department of Physics and Astronomy, Tel Aviv University, Tel Aviv 69978, Israel
[23]International Centre for Elementary Particle Physics and Department of Physics, University of Tokyo, Tokyo 113-0033, and Kobe University, Kobe 657-8501, Japan
[24]Particle Physics Department, Weizmann Institute of Science, Rehovot 76100, Israel
[25]Universität Hamburg/DESY, II Institut für Experimental Physik, Notkestrasse 85, D-22607 Hamburg, Germany
[26]University of Victoria, Department of Physics, P O Box 3055, Victoria BC V8W 3P6, Canada
[27]University of British Columbia, Department of Physics, Vancouver BC V6T 1Z1, Canada
[28]University of Alberta, Department of Physics, Edmonton AB T6G 2J1, Canada
[29]Research Institute for Particle and Nuclear Physics, H-1525 Budapest, P O Box 49, Hungary
[30]Institute of Nuclear Research, H-4001 Debrecen, P O Box 51, Hungary
[31]Ludwigs-Maximilians-Universität München, Sektion Physik, Am Coulombwall 1, D-85748

Garching, Germany
[32]Max-Planck-Institute für Physik, Föhring Ring 6, 80805 München, Germany
[33]Yale University,Department of Physics,New Haven, CT 06520, USA

[a] and at TRIUMF, Vancouver, Canada V6T 2A3
[b] and Royal Society University Research Fellow
[c] and Institute of Nuclear Research, Debrecen, Hungary
[e] and Heisenberg Fellow
[f] and Department of Experimental Physics, Lajos Kossuth University, Debrecen, Hungary
[g] and MPI München
[i] and Research Institute for Particle and Nuclear Physics, Budapest, Hungary
[j] now at University of Liverpool, Dept of Physics, Liverpool L69 3BX, UK
[k] and University of California, Riverside, High Energy Physics Group, CA 92521, USA
[l] and CERN, EP Div, 1211 Geneva 23
[m] and Tel Aviv University, School of Physics and Astronomy, Tel Aviv 69978, Israel.

1 Introduction

In the mid 1990's, the LEP collider at CERN entered a new phase of operation, LEP2, with the first e^+e^- collisions above the W^+W^- threshold. Between 1998 and 2000, with the installation of additional super-conducting radio-frequency accelerating cavities, the centre-of-mass energy of the LEP collider was further increased. The LEP2 data accumulated at centre-of-mass energies between 189 GeV and 209 GeV have opened up a new kinematic domain for particle searches.

The top quark mass was measured at the Tevatron collider to be $174.3 \pm 5.1\,\mathrm{GeV}/c^2$ [1, 2]. Due to this high mass, top quarks may only be singly produced at LEP2. Single top quark production in the Standard Model (SM) process $e^+e^- \to e^-\bar{\nu}_e t\bar{b}$ has a cross-section of about 10^{-4} fb at LEP2 energies [3] and can not be seen with the available luminosities. Another possible process for single top quark production is the flavour changing neutral current (FCNC) reaction[1]:

$$e^+e^- \to \bar{t}c(u). \tag{1}$$

Such FCNC are known to be absent at the tree level in the SM but can naturally appear at the one-loop level due to CKM mixing which leads to cross-sections of the order of 10^{-9} fb at LEP2 energies [4]. Extensions of the SM such as supersymmetry, exotic quarks, and multi-Higgs doublet models could lead to an enhancement of such transitions [5, 6, 7, 8]. In this paper the search for single top production via the FCNC reaction $e^+e^- \to \bar{t}c(u)$ is reported.

At the Tevatron, the CDF Collaboration performed a search for FCNC in the top decays $t \to \gamma\, c(u)$ and $t \to Z\, c(u)$ in $p\bar{p}$ collisions at a centre-of-mass energy of 1.8 TeV. They obtained upper limits at the 95% confidence level (CL) on the branching fractions [9]: $\mathrm{Br}(t \to c\gamma) + \mathrm{Br}(t \to u\gamma) < 3.2\%$ and $\mathrm{Br}(t \to cZ) + \mathrm{Br}(t \to uZ) < 33\%$.

The FCNC reaction can be described with the parameters κ_γ and κ_Z which represent the tree-level γ and Z exchange contributions to $e^+e^- \to \bar{t}c(u)$. Thus, the Born-level cross-section for single top production in e^+e^- collisions for $\sqrt{s} > m_t$ can be written as [6]:

$$\begin{aligned}\sigma[e^+e^- \to \bar{t}c(u)] = \frac{\pi\alpha^2}{s}\left(1-\frac{m_t^2}{s}\right)^2\Bigg[\kappa_\gamma^2 e_q^2 \frac{s}{m_t^2}\left(1+\frac{2m_t^2}{s}\right) \\ + \frac{\kappa_Z^2(1+a_w^2)(2+\frac{m_t^2}{s})}{4\sin^4 2\vartheta_W(1-\frac{m_Z^2}{s})^2} + 3\kappa_\gamma\kappa_Z\frac{a_w e_q}{\sin^2 2\vartheta_W(1-\frac{m_Z^2}{s})}\Bigg],\end{aligned} \tag{2}$$

where s is the centre-of-mass energy squared, α is the fine structure constant, $e_q = 2/3$ and m_t are the charge and mass of the top quark, m_Z is the Z boson mass, and $a_w = 1 - 4\sin^2\vartheta_W$ with ϑ_W being the weak-mixing angle. The three terms in Equation 2 correspond to the contribution from annihilation via a photon, a Z boson, and their interference. Using the published limits of CDF on FCNC, one can derive the following model-dependent limits at 95% CL [6, 9]: $\kappa_\gamma^2 < 0.176$ and $\kappa_Z^2 < 0.533$.

[1] Throughout this paper, charge conjugate states are implied.

In principle, a large FCNC coupling could not only lead to the associated production of a top plus a light quark at LEP2, but also to sizable branching ratios of the top quark into γc(u) or Zc(u). This analysis uses only the t $\rightarrow$ bW channel. The reduction of the branching ratio BR(t $\rightarrow$ bW) due to possible FCNC decays is taken into account in the results section.

2 Data and Monte Carlo Samples

The present analysis is based on data collected by the OPAL detector [10] from 1998 to 2000 at centre-of-mass energies between 189 GeV and 209 GeV. OPAL is a multipurpose high energy physics detector incorporating excellent charged and neutral particle detection and measurement capabilities. The search presented here uses 600.1 pb^{-1} of data collected at high energies for which the necessary detector components were required to be operational while the data were recorded. In addition, 11.3 pb^{-1} of calibration data were collected at $\sqrt{s} \sim m_{\mathrm{Z}}$ in 1998–2000 and have been used for fine tuning of the Monte Carlo simulation. In this paper, the data sample recorded in 1998 at $\sqrt{s} \simeq 189$ GeV is analysed in one bin, while the data from 1999 are divided into four samples at $\sqrt{s} \simeq$ 192, 196, 200 and 202 GeV. The data collected in 2000 is analysed in two samples of mean centre-of-mass energies of about 205 and 207 GeV.

A variety of Monte Carlo samples were generated for the evaluation of the detection efficiencies for single top production and SM background processes. In all samples, the hadronisation process is simulated with `JETSET` 7.4 [11] with parameters described in Reference [12] and the W boson mass is set to $m_{\mathrm{W}} = 80.33\,\mathrm{GeV}/c^2$. For each Monte Carlo sample, the detector response to the generated particles is simulated by a `GEANT3` based package [13].

The main Monte Carlo generator used for the description of our signal is `PYTHIA` [11], which produces $\bar{\mathrm{t}}$c(u) via an s-channel exchange of a Z boson. The top quark decays into a b quark and a W boson before it can form a bound state or radiate gluons. A colour string is formed between the $\bar{\mathrm{b}}$ and c(u) quarks to form a colour singlet. All couplings and quark fragmentation parameters for $\mathrm{e^+e^-} \rightarrow \bar{\mathrm{t}}$c(u) are set as in Z decays to quark pairs. For an evaluation of systematic errors associated with the Monte Carlo modelling, the signal is also modelled with a different `PYTHIA` process and the `EXOTIC` generator [14]. This other `PYTHIA` process is based on a model [15] for the production of a horizontal gauge boson, called R^0, with the decay $\mathrm{R}^0 \rightarrow \bar{\mathrm{t}}$c(u). The `EXOTIC` generator was developed for pair or single production of heavy and excited fermions. Here, the top quark is the heavy fermion and its production is associated with a c or u quark. A sequential decay model is assumed with all couplings to the known gauge bosons set to the SM expectations. For all three generators, samples for three different top quark masses (169, 174, and 179 GeV/c^2) have been generated. The signal Monte Carlo samples used for the reaction $\mathrm{e^+e^-} \rightarrow \bar{\mathrm{t}}$c(u) encompass a wide range of schemes for the form of the FCNC couplings, the angular distributions of the final state particles, and the parton shower parameters.

The background processes are simulated, with more statistics than the data collected, using the following event generators: `PYTHIA`, `KK2F` [16], and `HERWIG` [17] for $(\mathrm{Z}/\gamma)^* \rightarrow \mathrm{q\bar{q}}(\gamma)$; grc4f [18], `KORALW` [19], and `EXCALIBUR` [20] for four-fermion (4f) processes; and `HERWIG`, `PHOJET` [21], and `Vermaseren` [22] for two-photon scattering.

3 Event Selection

The searches for single top events $e^+e^- \to \bar{t}c(u) \to \bar{b}Wc(u)$ are sensitive to the leptonic and hadronic decays of the W boson: $W \to \ell\bar{\nu}_\ell$ and $W \to q\bar{q}$. The leptonic channel is a clean final state with specific topology and kinematics; it is characterised by two hadronic jets, one isolated lepton, some missing energy (carried away by the neutrino), and the presence of a b-hadron decay. While the hadronic channel is not as clean as the leptonic channel, it is statistically significant because BR(W $\to$ hadron) $\approx$ 68% and BR(W $\to \ell\bar{\nu}_\ell$) $\approx$ 32% ($\ell = e$, μ, and τ). The hadronic channel is characterised by four hadronic jets with specific topology and kinematics, large visible energy, and the presence of a b-hadron decay. Common search procedures are applied to both channels. The event selection begins with loose global preselection criteria designed to remove most of the two-photon and low multiplicity events. To obtain optimal resolution for single top candidates, kinematic fits are performed to reject badly reconstructed events and background which are not compatible with the topology of single top events. Consequently, the event selection is followed by detailed preselection cuts for both the leptonic and the hadronic channels. The final candidate events are then identified using relative likelihood functions. Each step will be described briefly in the following subsections.

3.1 Global Event Selection Criteria

Events are reconstructed from tracks in the central tracking system and energy clusters in the electromagnetic and hadron calorimeters, using selection criteria which are the same as those used for the OPAL Higgs analysis [23]. Because of the presence of jets in a single top event, general multi-hadronic preselections are applied. Each event must qualify as a multi-hadronic final state according to the criteria of References [24, 25]. These cuts remove events with low multiplicity or little visible energy and reject effectively two-photon and pure leptonic events.

The final state particles and clusters are grouped into jets using the Durham algorithm [26]. These jets are used as reference jets in the following assignment procedure. In calculating the visible energies and momenta, E_{vis} and $\vec{p}_{vis}$, of the event and of individual jets, corrections are applied to prevent double-counting of the energy of the tracks and their associated clusters [27].

3.2 Lepton Identification

Lepton identification for the leptonic channel relies primarily on the isolation criteria of a prompt charged particle. Isolated leptons are identified using the Neural Network (NN_ℓ) described in Reference [28]. The NN_ℓ uses all tracks in an event with $|\vec{p}| > 2$ GeV/c which are considered one-by-one in decreasing order of momentum. They are used as seed tracks and all tracks and unassociated clusters within 10° of the seed track define the lepton. Afterward the leptons are classified as one-prong or three-prong candidates depending on the number of tracks within the 10° cone. Around the seed candidate an annular cone of 30° is drawn concentric with and excluding the 10° narrow cone. This serves to define the isolation criteria of the lepton candidate. The NN_ℓ provides a distinctive signature for high energy leptons

from the particle flow in the annular and narrow cones. However, this procedure is flavour blind; the main interest is to retain high identification efficiency. Thus, the NN_ℓ topological identification is sensitive to the detection of electrons, muons, and taus with efficiencies of 84%, 84%, and 75%, respectively. The probability of misidentifying a hadron from a parton shower as a lepton is around 1% for $\mathrm{NN}_\ell > 0.75$. The main source of misidentified leptons comes from low-multiplicity gluon jets.

The lepton with the largest NN_ℓ output in every event is taken to be the lepton of the $\bar{\mathrm{t}} \to \bar{\mathrm{b}}\mathrm{W} \to \bar{\mathrm{b}}\,\ell\bar{\nu}_\ell$ decay. In order to improve the performance of the kinematic fits, a simple identification is used to determine the mass (flavour) of the lepton candidate. First, all three-prong candidates are classified as taus. Then, a lepton is classified as an electron if $\mathcal{P}_e \geq 0.5$, $E_\ell > 20\,\mathrm{GeV}$, and $\cos\theta_{\ell-\nu} < 0.25$, where $\mathcal{P}_e$ is the standard OPAL electron identification probability [29], E_ℓ is the energy of the lepton, and $\theta_{\ell-\nu}$ is the opening angle between the lepton and the missing momentum vector. Of the remaining leptons, the candidates with $\mathcal{P}_e < 0.5$, $E_\ell > 20\,\mathrm{GeV}$, and $\cos\theta_{\ell-\nu} < 0.25$ are classified as muons, while the others are labelled as taus.

3.3 Event Kinematics

At a centre-of-mass energy of $\sqrt{s} \approx 189$ GeV the top quark is produced close to threshold. As the top quark is nearly at rest, the W boson in the $\mathrm{e^+e^-} \to \bar{\mathrm{t}}\mathrm{c(u)} \to \bar{\mathrm{b}}\mathrm{Wc(u)}$ reaction has almost constant energy $E_\mathrm{W} \simeq (m_\mathrm{t}^2 + m_\mathrm{W}^2 - m_\mathrm{b}^2)/2\,m_\mathrm{t}$, which also leads to fixed energy for the b quark $E_\mathrm{b} \simeq (m_\mathrm{t}^2 - m_\mathrm{W}^2 + m_\mathrm{b}^2)/2\,m_\mathrm{t}$. With increasing centre-of-mass energy this unique kinematic signature gets diluted.

These specific kinematic properties are exploited by using kinematic fits. First, the event is constrained to pass a 4C kinematic fit which ensures that the energy and momentum are conserved[2]. The 4C kinematic fit is employed to remove badly reconstructed events and events with missing particles along the beam pipe. The χ^2 probability of the 4C fit is thus required to be larger than 10^{-5}.

To obtain optimal resolution for the reconstructed candidates and performance for the jet assignment, we use additional kinematic fits which enforce energy and momentum conservation and impose the appropriate mass constraints. These fits are referred to as the 6C fits with the $\bar{\mathrm{t}}\mathrm{c(u)}$ or the WW hypothesis:

- $\mathbf{e^+e^- \to \bar{t}c(u) \to \bar{b}Wc(u)}$**:** W boson and top quark invariant mass constraints.
- $\mathbf{e^+e^- \to WW}$**:** two W boson invariant mass constraints.

In the 6C kinematic fits the W mass and the top quark mass are fitted with a soft constraint, approximating the Breit-Wigner shapes by Gaussian resolution functions. As for the 4C fit, we still refer any mass constrained fit as a 6C fit for $\bar{\mathrm{b}}\,\ell\bar{\nu}_\ell\,\mathrm{c(u)}$ events. To ensure that the kinematic properties of the event candidates match our signal process, we require $\mathcal{P}(6\mathrm{C}) > 10^{-5}$ for the $\bar{\mathrm{t}}\mathrm{c(u)}$ 6C fit.

[2]For semileptonic events, there are three unmeasured variables corresponding to the neutrino momentum so that the effective number of constraints in the leptonic mode is one. Nevertheless, any fit which implies that energy and momentum are conserved for both the leptonic and hadronic channels will be referred to as a 4C fit.

3.4 B-Tagging

The dominant background in this analysis comes from WW events. In $e^+e^- \rightarrow$WW events, the only heavy quark commonly produced is the charm quark. The production of bottom quarks is highly suppressed due to the small magnitude of $|V_{ub}|$ and $|V_{cb}|$ and the large mass of the top quark. Furthermore, since the top quark is expected to decay into a bW pair, the tagging of jets originating from b quarks plays an important role in single top production searches. The jet-wise b-tagging algorithm, which has been developed for the Higgs boson search, uses three independent b-tagging methods: (1) lifetime tag, (2) high-p_T lepton tag, and (3) jet shape tag. These three methods are combined using an unbinned likelihood method to form a single discriminating variable for each jet [28]. The b-tag becomes important for higher centre-of-mass energies because the kinematic situation changes and the signal is less well separated from the WW background.

3.5 Jet Assignment

In the hadronic channel, the correct assignment of particles to jets plays an essential role in reducing four-jet like backgrounds. There are twelve possible combinations to assign two jets to the W boson, the third jet to the $\bar{b}$ quark, and the fourth jet to the light flavoured quark. Therefore a discriminating variable is calculated, which is a combination of the 6C kinematic fit probability and the b-tag variable, in order to find the best matching combination to the signal hypothesis. The 6C fit helps to identify the two jets coming from the W and to find the third jet which matches kinematically to form the invariant top quark mass. In addition the b-tag variable helps to identify if this latter jet is a b-jet. The jet assignment which yields the largest $\mathcal{P}(\text{b-tag}, 6\text{C})$ is used to choose the jet/quark assignment. $\mathcal{P}(\text{b-tag}, 6\text{C})$ is calculated as:

$$\mathcal{P}(\text{b-tag}, 6\text{C}) = \frac{\mathcal{P}(6\text{C})\,\mathcal{P}(\text{b-tag})}{\mathcal{P}(6\text{C})\,\mathcal{P}(\text{b-tag}) + [1-\mathcal{P}(6\text{C})]\,[1-\mathcal{P}(\text{b-tag})]},$$

where $\mathcal{P}(\text{b-tag})$ is the b-tag variable and $\mathcal{P}(6\text{C})$ is the probability from the $\bar{t}c(u)$ 6C fit.

In the leptonic channel, the correct jet/quark assignment plays an important role in reducing signal-like background topology. In $e^+e^- \rightarrow \bar{t}c(u) \rightarrow \bar{b}\,\ell\bar{\nu}_\ell\,c(u)$, there are only two possible jet assignments. One of the jets must come from the hadronisation of the $\bar{b}$ quark and the other from the light flavoured quark. The bottom jet is taken to be the one with the largest $\mathcal{P}(\text{b-tag}, 6\text{C})$ from the $\bar{t}c(u)$ 6C fit.

With the jet assignment method described here, a Monte Carlo study shows that the rate of correct b-jet (non b-jet) assignment at $\sqrt{s} = 189\,\text{GeV}$ is about 96% (94%) and 84% (73%) for the leptonic and hadronic channels, respectively.

3.6 Single Top Candidate Preselection

To help further reduce the background after the global event selections, the kinematic fits, the b-tagging, and the jet assignment, individual preselection criteria are enforced for both the leptonic and the hadronic channels.

3.6.1 Preselection: Leptonic Channel

The following preselection cuts are applied in order to reduce background with a different topology to our signal process:

1. $N_{\rm lepton} \geq 1$, where $N_{\rm lepton}$ is the number of lepton candidates as described in Section 3.2.
2. $|\cos\theta_{\rm miss}| < 0.9$, where $|\cos\theta_{\rm miss}|$ is the cosine of the polar angle of the missing momentum vector. This cut rejects a large portion of the $\rm q\bar{q}(\gamma)$ background.
3. $M_{\rm vis}/\sqrt{s} > 0.20$, where $M_{\rm vis}$ is the invariant mass calculated from the visible energy $E_{\rm vis}$ and the visible momentum $\vec{p}_{vis}$ of the event.
4. $|\vec{p}_{miss}|/\sqrt{s} < 0.50$, where $\vec{p}_{miss}$ is calculated from the visible momentum ($\vec{p}_{miss} = -\vec{p}_{vis}$). This cut reject events with large missing momentum, such as $\rm q\bar{q}(\gamma)$ background when the photon escapes detection.
5. $0.20 < \sum|\vec{p}_{\rm T}|/\sqrt{s} < 0.90$, where $\sum|\vec{p}_{\rm T}|$ is the scalar sum of the transverse momentum components for all the good tracks and unassociated clusters. This cut prevents the visible momentum being toward the beam direction and rejects non-radiative $\rm q\bar{q}$ events with no missing energy.
6. $\rm NN_\ell > 0.75$, where $\rm NN_\ell$ is the primary lepton Neural Network output as described in Section 3.2.

After the preselection the background is well described by 4f and $\rm q\bar{q}$ events. Other final states, such as two-photon events, are negligible. The main background (around 95%) is due to $\rm WW \to q\bar{q}\ell\bar{\nu}_\ell$ events. The fraction of events with four quarks in the final state selected with the leptonic preselection criteria is negligible.

3.6.2 Preselection: Hadronic Channel

The following preselection cuts are applied in order to select only four-jet like events:

1. The event must contain at least 15 charged tracks.
2. The maximum energy of any electron or muon found in the event (identified as described in Reference [30]) must be less than 40 GeV.
3. The radiative process $\rm e^+e^- \to (Z/\gamma)^*\gamma \to q\bar{q}\gamma$ is reduced by requiring that the effective centre-of-mass energy $\sqrt{s'}$ [25] be at least 150 GeV.
4. The Durham jet resolution parameter y_{34}, at which the number of jets changes from three to four, is required to be larger than 0.001.
5. The $\rm (Z/\gamma)^* \to q\bar{q}$ background is further suppressed by requiring that the event shape parameter C [31], which is close to one for spherical events, is larger than 0.4.

After the preselection the background is well described by 4f and $\rm q\bar{q}$ events. The expected background is composed of 41% (70%) of 4f and 59% (30%) of $\rm q\bar{q}$ processes at $\sqrt{s} \simeq 189$ (207) GeV. Other final states, such as two-photon events, are negligible. The fraction of $\rm q\bar{q}\ell\bar{\nu}_\ell$ events selected by the hadronic preselection criteria is less than 1%.

3.7 Likelihood Selection

The final separation of the signal from the background is achieved with a conventional multi-variable relative likelihood function [32]:

$$\mathcal{L} = \frac{\mathcal{P}_{\text{signal}}}{\mathcal{P}_{\text{signal}} + \mathcal{P}_{\text{background}}}, \quad \text{with} \quad \mathcal{P} = \prod_i p_i.$$

The template (or reference) histograms of the input variables, p_i, are used as the probability density functions for the calculation of $\mathcal{P}_{\text{signal}}$ and $\mathcal{P}_{\text{background}}$. We rely on Monte Carlo events to compute the probability density functions.

3.7.1 Likelihood: Leptonic Channel

For each event satisfying the $\mathrm{q\bar{q}}\ell\bar{\nu}_\ell$ preselection cuts, a binned likelihood function is constructed, with one class for the signal and one for the 4f background. The relative likelihood is calculated using the following variables:

$\boldsymbol{E_{c(u)}}$**:** The energy of the light flavoured jet.

$\boldsymbol{M_{qq}^{4C}}$**:** The invariant mass of the $\mathrm{q\bar{q}}$ system after the 4C fit.

$\boldsymbol{M_{\ell\nu} = \sqrt{E_{\text{beam}}^2 - (\vec{p}_{\ell\nu}^{\,4C})^2}}$**:** Pseudo mass of the $\ell\bar{\nu}_\ell$ system after the 4C fit, calculated from the beam energy and the momentum of the $\ell\bar{\nu}_\ell$ pair.

$\boldsymbol{\ln y_{12}}$**:** The logarithm of the Durham jet resolution parameter at which the number of reconstructed jets passes from one to two.

$\boldsymbol{M_{qq}^{6C} + M_{\ell\nu}^{6C}}$**:** The sum of the di-jet and $\ell\bar{\nu}_\ell$ invariant masses for the 6C fit under the WW hypothesis.

b-tag: The b-tag variable of the selected bottom jet.

$\boldsymbol{\mathcal{P}}$**(b-tag, 6C):** The discriminant variable which combines the b-tag variable and the $\bar{\mathrm{t}}\mathrm{c(u)}$ 6C fit probability.

Jets tagged as light flavoured jets in the background from SM processes have much higher values of $E_{c(u)}$. The second and third variables offer good discrimination for $\mathrm{WW} \to \mathrm{q\bar{q}}\ell\bar{\nu}_\ell$ events since they exploit the specific angular distribution of signal events. The variable y_{12} exploits the unique jet distribution in $\bar{\mathrm{t}}\mathrm{c(u)}$ events. To further remove the background from semileptonic WW decays, we use $M_{qq}^{6C} + M_{\ell\nu}^{6C}$. Finally, we use the b-tag variable and the $\mathcal{P}(\text{b-tag}, 6\text{C})$ of the b-jet to separate bottom-less events. Figure 1 shows the distributions of the input variables for data, the SM background, and the simulated single top signal at $\sqrt{s} = 189\,\text{GeV}$. There is good agreement between data and Monte Carlo distributions from background processes.

3.7.2 Likelihood: Hadronic Channel

For each event satisfying the $q\bar{q}q\bar{q}$ preselection cuts, a binned likelihood function is constructed, with one class for the signal and two for the $q\overline{q}q\overline{q}$ and the $q\bar{q}$ backgrounds. The relative likelihood is calculated using the following variables:

χ^2(6C fit): The χ^2 of the $\bar{t}c(u)$ 6C kinematic fit.

$E_{c(u)}/E_{vis}$: The ratio of the energy of the c(u) jet and the total visible energy.

Thrust: The value of the thrust for the event [11].

b-tag: The b-tag variable of the selected bottom jet.

cos($\angle(\vec{p}_{Wq1}, \vec{p}_{Wq2})$): The cosine of the angle between the two jets tagged as decay products of the W boson.

The thrust variable exploits the different event topologies between signal and backgrounds. The b-tag variable is used as an effective likelihood input because the top quark is expected to decay into a b quark. The other three variables exploit the specific kinematics of signal events. Figure 2 shows the distributions of the input variables for data, the SM background, and the simulated single top signal at $\sqrt{s} = 189\,\text{GeV}$. There is good agreement between data and Monte Carlo distributions from background processes.

3.7.3 Likelihood: Both Channels

In Figure 3 the relative likelihood functions for the leptonic and hadronic channels are shown for data collected at $\sqrt{s} \simeq 205$ - $207\,\text{GeV}$ and for the SM expectation. No excess of events is observed. The likelihood functions for FCNC signal events for an assumed arbitrary cross-section of 3 pb are also depicted in Figure 3. It can be seen that the expected signal contribution is concentrated at high values of $\mathcal{L}$.

There is no evidence of single top quark production in the data for any $\sqrt{s}$. Thus, the final likelihood cuts are chosen at each value of $\sqrt{s}$ so as to minimise the expected upper limit on the signal cross-section and thus to maximise the expected exclusion sensitivity. The number of selected data and expected SM background events as a function of the centre-of-mass energies are shown in Table 1.

4 Systematic Errors

4.1 Signal Efficiencies and SM Backgrounds

Sources of systematic uncertainties are investigated for their effect on the signal detection efficiencies and the SM backgrounds. They are listed in Table 2 for three of the energy bins and are discussed below. All checks were performed for all centre-of-mass energies. Possible color reconnection and Bose-Einstein effects were not investigated.

The errors on the background and signal rates from the modelling of the preselection variables and of the detector response are a few percent. These uncertainties are evaluated

Label (GeV)	$\sqrt{s}$ (GeV)	Lumi. (pb^{-1})	Leptonic Channel		Hadronic Channel	
			Data	SM Total	Data	SM Total
189	188.7	172.1	3	4.0	13	11.6
192	191.6	28.9	0	1.0	7	5.1
196	195.6	74.8	1	2.9	6	6.4
200	199.6	77.2	3	2.7	10	9.4
202	201.6	36.1	2	1.2	8	7.5
205	205.1	80.3	1	2.0	11	10.1
207	206.8	130.8	6	3.8	14	16.4

Table 1: The luminosity-weighted mean centre-of-mass energies, the integrated luminosities, the number of selected data and expected SM background events at $\sqrt{s} = 189$ - 209 GeV are shown for the leptonic and hadronic channels.

based on comparisons of the distributions of the variables in the calibration data collected at $\sqrt{s} \sim m_{\mathrm{Z}}$ and the Monte Carlo simulation. The effects of detector mis-calibration and deficiencies were investigated by varying the jet and lepton energy scales over a reasonable range [33]. The uncertainties on the energy resolution and the angular resolution were also evaluated, but have much smaller effects. A comparison of alternative Monte Carlo generators for the background accounts for an additional uncertainty on the background rates. The difference between the luminosity-weighted centre-of-mass energies in data and the value of $\sqrt{s}$ used in the main Monte Carlo samples results in an additional uncertainty on the background and signal selection efficiencies due to the use of an energy constraint in the kinematic fits. Lepton identification accounts for an extra uncertainty for the leptonic channel.

One of the dominant errors in both analysis channels arises from the b-tagging. Recent improvements in the knowledge of heavy quark production processes and decays, such as the b-hadron charged decay multiplicity and the gluon splitting rate to heavy quarks, are taken into account in the analysis by reweighting Monte Carlo events [34]. The sensitivity to the b-vertex reconstruction was assessed by degrading or improving the tracking resolution in the Monte Carlo. It was found that changing the track parameter resolutions by $\pm 5\%$ in the Monte Carlo simulation covers the range of possible differences between data and simulated events. Overall it leads to an uncertainty of 3.8-8.4% for the b-tag rates of background and signal events. The finite size of the Monte Carlo samples used in this analysis results in an additional uncertainty of a few percent for the background and the signal selection efficiencies.

All the different systematic effects for the background and the signal efficiencies are treated as being independent. The total uncertainties on the background and signal rates, for both the leptonic and the hadronic channel, are in the same range and show small dependencies on the centre-of-mass energy. For each centre-of-mass energy, the systematic errors are included in the calculation of the cross-section upper limits.

Source of Systematic Error	Leptonic Channel		Hadronic Channel	
	Δefficiency	Δbackground	Δefficiency	Δbackground
Preselection	1.0/1.4/1.2	2.0/2.2/1.9	1.0/0.4/0.3	3.2/1.4/0.5
Detector Response	1.0/2.2/3.4	1.4/1.7/1.2	0.6/2.0/1.5	1.0/1.0/3.0
Background	- / - / -	6.8/7.4/6.9	- / - / -	5.0/5.0/5.0
$\sqrt{s}$ in MC	1.1/2.4/1.9	2.7/2.1/2.3	0.6/0.8/0.5	1.5/1.3/1.4
Lepton ID	4.4/5.0/4.8	3.0/4.0/3.5	- / - / -	- / - / -
b-tagging	4.2/6.6/5.2	7.8/5.6/7.0	3.8/5.3/5.2	6.9/5.5/8.4
MC Statistic	2.2/2.3/2.1	1.5/2.0/1.6	2.0/1.8/1.8	5.4/5.0/4.8
FCNC modelling	7.2/8.3/3.5	- / - / -	7.9/6.6/5.0	- / - / -
Total	9.8/12.5/9.1	11.5/10.9/11.0	9.1/8.9/7.6	10.7/9.2/11.4

Table 2: The relative systematic errors (in %) on the signal reconstruction efficiency and on the background modelling for $\sqrt{s}$ = 189/200/207 GeV.

4.2 FCNC Modelling

Several methods of producing FCNC can be compared. A comparison of the results obtained with the `EXOTIC` and the `PYTHIA` samples described in Section 2 allows an estimate of the uncertainty due to the model used for the signal process. The difference is taken as a modelling uncertainty on the simulation of signal events. It is summarised in Table 2. The main disparities between all the generator schemes are the angular distributions of the particles produced in the final state and the parton shower modelling of the initial quarks. This latter effect gives rise to one of the largest uncertainties on the signal reconstruction efficiency.

4.3 Top Quark Mass

The largest systematic uncertainty comes from the sensitivity of the event selection to the assumed value of the top quark mass. In the analysis we assume the mass of the top quark to be 174 GeV/c^2. To take this dependency into account, the variation of the reconstruction efficiency is investigated using Monte Carlo events with m_{t}= 169 and 179 GeV/c^2 incorporating the experimental systematic and the FCNC model uncertainties described in the previous sections. The dependence of the reconstruction efficiencies on the top quark mass for the leptonic and hadronic channels is summarised in Table 3.

5 Results

No evidence for single top quark production is observed in $\mathrm{e^+e^-}$ collisions at centre-of-mass energies between 189-209 GeV. Limits on the single top cross-section have been derived at the 95% CL from the measurements of the number of observed events, the reconstruction efficiencies, and the integrated luminosities [35]. The upper limit calculations for each individual centre-of-mass energy are summarised in Table 3. Those results include both the

$\sqrt{s}$	$m_{\rm t} = 169\,{\rm GeV}/c^2$			$m_{\rm t} = 174\,{\rm GeV}/c^2$			$m_{\rm t} = 179\,{\rm GeV}/c^2$		
(GeV)	ϵ_ℓ	ϵ_q	$\sigma_{95}^{\rm obs.}$	ϵ_ℓ	ϵ_q	$\sigma_{95}^{\rm obs.}$	ϵ_ℓ	ϵ_q	$\sigma_{95}^{\rm obs.}$
189	7.5	10.3	0.30	9.1	12.8	0.24	6.1	10.0	0.33
192	7.5	15.3	0.99	9.5	18.0	0.81	6.9	14.9	1.04
196	7.1	12.8	0.39	8.7	14.7	0.33	7.2	12.1	0.40
200	7.1	14.7	0.55	8.0	16.0	0.50	7.0	15.1	0.55
202	6.6	17.7	1.00	7.5	18.6	0.93	6.9	17.3	1.00
205	5.9	14.4	0.48	7.0	15.7	0.43	6.2	13.9	0.49
207	5.8	12.8	0.47	6.7	15.4	0.40	6.1	13.6	0.45

Table 3: The reconstruction efficiencies for the leptonic (ϵ_ℓ) and the hadronic (ϵ_q) channels are shown. The overall measured 95% CL upper limits on single top production cross-section ($\sigma_{95}^{\rm obs.}$) are reported. The statistical and systematic uncertainties are included in the calculation of the upper limits. The efficiencies (in %) and the limits on the cross-section (in pb) are shown as a function of the centre-of-mass energy for $m_{\rm t} = 169$, 174, and $179\,{\rm GeV}/c^2$. These results assume a 100% branching fraction of the top quark into b W.

statistical and systematic errors and are valid under the assumption that $m_{\rm t} = 169$, 174, and $179\,{\rm GeV}/c^2$ and that BR(t $\rightarrow$ b W) = 100%. The CDF limits constrain the t $\rightarrow V$c(u) FCNC branching ratio to be smaller than about 36% [9] for $V = \gamma$ or Z, so that in a pessimistic scenario the OPAL efficiencies and cross-section limits quoted in Table 3 should be rescaled by 64%.

The combination of all the data can be used to determine limits on the anomalous coupling parameters κ_γ and $\kappa_{\rm Z}$. First, the QCD and the ISR effects which modify the Born-level cross-section given in Equation 2 must be considered. The QCD correction is taken from Section 3 of Reference [36]; while the ISR correction is based on Reference [37]. Overall, the QCD and ISR corrections increase the Born-level cross-section by a constant factor of about 1.09 for all centre-of-mass energies and produce only a small distortion to the OPAL exclusion region in the $\kappa_\gamma - \kappa_{\rm Z}$ plane.

The limits on the anomalous coupling parameters are obtained with the likelihood ratio method described in Reference [35]. Each centre-of-mass energy for the leptonic and the hadronic channel has been used as an independent channel. The variation of the selection efficiencies for different top masses are taken from Table 3. Taking the statistical and systematic errors into account the limit on the anomalous coupling parameters in the $\kappa_\gamma - \kappa_{\rm Z}$ plane have been derived at the 95% CL. The reduction of the branching ratio BR(t $\rightarrow$ bW) due to possible FCNC decays derived at each point in the $\kappa_\gamma - \kappa_{\rm Z}$ plane is taken into account in this generic FCNC production limit calculation. To compare our results with the limits from CDF, exclusion regions for $m_{\rm t} = 169$, 174, and $179\,{\rm GeV}/c^2$ in the $\kappa_\gamma - \kappa_{\rm Z}$ plane were obtained. The results are shown in Figure 4. They correspond to upper limits of $\kappa_\gamma < 0.48$ and $\kappa_{\rm Z} < 0.41$ for a top quark mass of $m_{\rm t} = 174\,{\rm GeV}/c^2$, which becomes $\kappa_\gamma < 0.39$ (0.60) and $\kappa_{\rm Z} < 0.34$ (0.52) for $m_{\rm t} = 169$ (179) ${\rm GeV}/c^2$. These exclusions translate into branching fraction limits of Br(t $\rightarrow$ Zc) + Br(t $\rightarrow$ Zu) < 9.7/13.7/20.6 % for $m_{\rm t} = 169/174/179\,{\rm GeV}/c^2$. All these results are consistent with recent results from the ALEPH Collaboration [38].

6 Summary

A search for single top quark production via FCNC has been performed with 600.1 pb^{-1} of data collected by OPAL in $\mathrm{e}^+\mathrm{e}^-$ collision at $\sqrt{s}$ = 189 - 209 GeV. In total, 85 events were selected in the data with a SM expectation of 84.1 events. Limits on single top quark cross-sections have been derived at the 95% CL. This leads to model-dependent upper limits of κ_γ <0.48 and κ_Z <0.41 for a top quark mass of m_t = 174 GeV/c^2. The limits become κ_γ <0.39 (0.60) and κ_Z <0.34 (0.52) for m_t = 169 (179) GeV/c^2.

Acknowledgements:

We particularly wish to thank the SL Division for the efficient operation of the LEP accelerator at all energies and for their close cooperation with our experimental group. We thank our colleagues from CEA, DAPNIA/SPP, CE-Saclay for their efforts over the years on the time-of-flight and trigger systems which we continue to use. In addition to the support staff at our own institutions we are pleased to acknowledge the
Department of Energy, USA,
National Science Foundation, USA,
Particle Physics and Astronomy Research Council, UK,
Natural Sciences and Engineering Research Council, Canada,
Israel Science Foundation, administered by the Israel Academy of Science and Humanities,
Minerva Gesellschaft,
Benoziyo Center for High Energy Physics,
Japanese Ministry of Education, Science and Culture (the Monbusho) and a grant under the Monbusho International Science Research Program,
Japanese Society for the Promotion of Science (JSPS),
German Israeli Bi-national Science Foundation (GIF),
Bundesministerium für Bildung und Forschung, Germany,
National Research Council of Canada,
Research Corporation, USA,
Hungarian Foundation for Scientific Research, OTKA T-029328, T023793 and OTKA F-023259.

References

[1] CDF Collaboration, F. Abe *et al.*, Phys. Rev. Lett. **82** (1999) 271;
D0 Collaboration, B. Abbott *et al.*, Phys. Rev. **D60** (1999) 012001;
L. Demortier *et al.*, FERMILAB-TM-2084 (1999).

[2] Particle Data Group, C. Caso *et al.*, Eur. Phys. J. **C3** (1998) 1;
Particle Data Group, D.E. Groom *et al.*, Eur. Phys. J. **C15** (2000) 1.

[3] O. Panella, G. Pancheri and Y.N. Srivastava, Phys. Lett. **B318** (1993) 241;
K. Hagiwara, M. Tanaka and T. Stelzer, Phys. Lett. **B325** (1994) 521;
E. Boos *et al.*, Phys. Lett. **B326** (1996) 190.

[4] C.-S. Huang, X.-H. Wu and S.-H. Zhu, Phys. Lett. **B425** (1999) 143.

[5] H. Fritzsch, D. Holtmannspötter, Phys. Lett. **B457** (1999) 186.

[6] J.F. Obraztsov, S. Slabospitsky, O. Yushchenko, Phys. Lett. **B426** (1998) 393.

[7] T. Han, J.L. Hewett, Phys. Rev. **D60** (1999) 074015.

[8] F. del Aguila, J.A. Aguilar-Saavedra and R. Miquel, Phys. Rev. Lett. **82** (1999) 1628.

[9] CDF Collaboration, F. Abe *et al.*, Phys. Rev. Lett **80** (1998) 2525.

[10] OPAL Collaboration, K. Ahmet *et al.*, Nucl. Instr. Meth. **A305** (1991) 275;
OPAL Collaboration, P.P. Allport *et al.*, Nucl. Instr. Meth. **A324** (1993) 34;
OPAL Collaboration, P.P. Allport *et al.*, Nucl. Instr. Meth. **A346** (1994) 476;
OPAL Collaboration, S. Anderson *et al.*, Nucl. Instr. Meth. **A403** (1998) 326.

[11] T. Sjöstrand, Comp. Phys. Comm. **82** (1994) 74;
T. Sjöstrand, LU TP 95-20.

[12] OPAL Collaboration, G. Alexander *et al.*, Z. Phys **C69** (1996) 543.

[13] J. Allison *et al.*, Nucl. Inst. and Meth. **A317** (1992) 47.

[14] A. Djouadi, Z. Phys. **C63** (1994) 317;
F. Boudjema, A. Djouadi, and J.L. Kneur, Z. Phys. **C57** (1993) 425;
R. Tafirout and G. Azuelos, Comp. Phys. Comm. **126** (2000) 244.

[15] H.-U. Bengtsson *et al.*, Phys. Rev. Lett. **55** (1985) 2762.

[16] S. Jadach, B.F. Ward and Z. Was, Phys. Lett. **B449** (1999) 97.

[17] G. Marchesini *et al.*, Comp. Phys. Comm. **67** (1992) 465.

[18] J. Fujimoto *et al.*, Comp. Phys. Comm. **100** (1997) 128;
J. Fujimoto *et al.*, *Physics at LEP2*, CERN 96-01 (1996), Vol.2, 30.

[19] M. Skrzypek *et al.*, Comp. Phys. Comm. **94**(1996) 216;
M. Skrzypek *et al.*, Phys. Lett. **B372** (1996) 289.

[20] F.A. Berends, R. Pittau, and R. Kleiss, Comp. Phys. Comm. **85** (1995) 437.

[21] R. Engel and J. Ranft, Phys. Rev. **D54** (1996) 4244;
R. Engel, Z. Phys **C66** (1995) 203.

[22] J.A.M. Vermaseren, Nucl. Phys. **B229** (1983) 347.

[23] OPAL Collaboration, R. Akers *et al.*, Phys. Lett. **B327** (1994) 397.

[24] OPAL Collaboration, G. Alexander *et al.*, Z. Phys **C52** (1991) 175.

[25] OPAL Collaboration, K. Ackerstaff *et al.*, Eur. Phys. J. **C2** (1998) 441.

[26] N. Brown and W.J. Stirling, Phys. Lett. **B252** (1990) 657;
S. Catani *et al.*, Phys. Lett. **B269** (1991) 432;
N. Brown and W.J. Stirling, Z. Phys. **C53** (1992) 629.

[27] OPAL Collaboration, M.Z. Akrawy *et al.*, Phys. Lett. **B253** (1990) 511;
OPAL Collaboration, K. Ackerstaff *et al.*, Eur. Phys. J. **C2** (1998) 213.

[28] OPAL Collaboration, G. Abbiendi *et al.*, Eur. Phys. J. **C7** (1999) 407.

[29] OPAL Collaboration, G. Alexander *et al.*, Z. Phys. **C70** (1996) 357;
OPAL Collaboration, G. Abbiendi *et al.*, Eur. Phys. J. **C8** (1999) 217.

[30] OPAL Collaboration, K. Ackerstaff *et al.*, Eur. Phys. J. **C1** (1998) 425.

[31] G. Parisi, Phys. Lett. **B74** (1978) 65;
J.F. Donoghue, F.E. Low and S.Y. Pi, Phys. Rev. **D20** (1979) 2759.

[32] D. Karlen, Comp. in Phys. **12** (1998) 380.

[33] OPAL Collaboration, G. Abbiendi *et al.*, Phys. Lett. **B507** (2001) 29.

[34] OPAL Collaboration, G. Abbiendi *et al.*, Phys. Lett. **B499** (2001) 38.

[35] T. Junk, Nucl. Inst. and Meth. **A434** (1999) 435.

[36] L.J. Reinders *et al.*, Physics Reports, **127** (1985) 1.

[37] F.A Berends and R. Kleiss, Nucl. Phys. **B260** (1985) 32.

[38] ALEPH Collaboration, R. Barate *et al.*, Phys. Lett. **B494** (2000) 33.

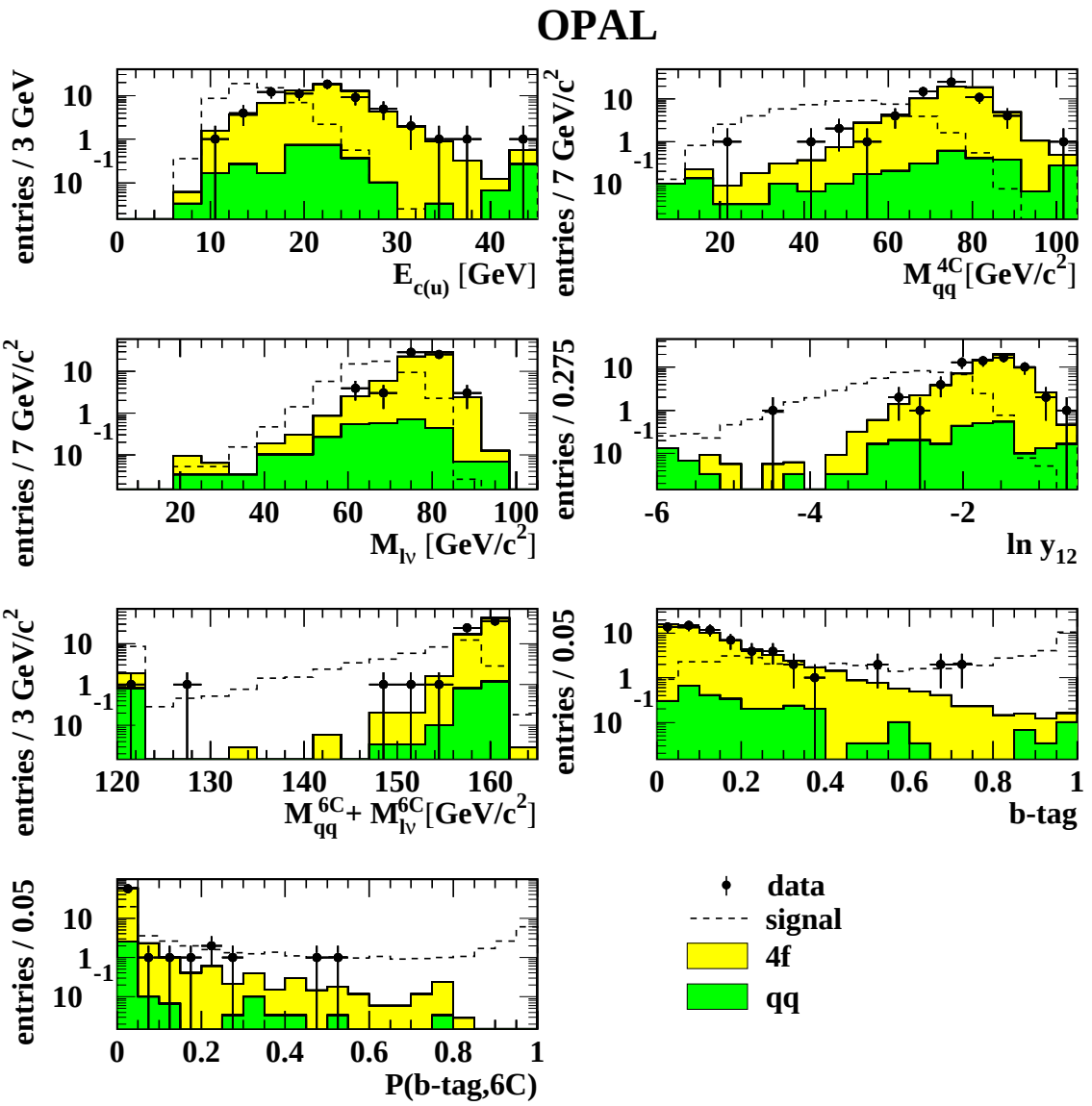

Figure 1: Distributions of the likelihood variables for the leptonic channel at $\sqrt{s} \simeq 189\,\mathrm{GeV}$. Comparisons between the data, the SM 4-fermion (light grey), and $\mathrm{q\bar{q}}$ backgrounds (grey) are shown. The dashed line represents single top MC events with $m_{\mathrm{t}} = 174\,\mathrm{GeV/c^2}$ and an arbitrary cross-section of $\sigma_{\mathrm{top}} = 3\,\mathrm{pb}$.

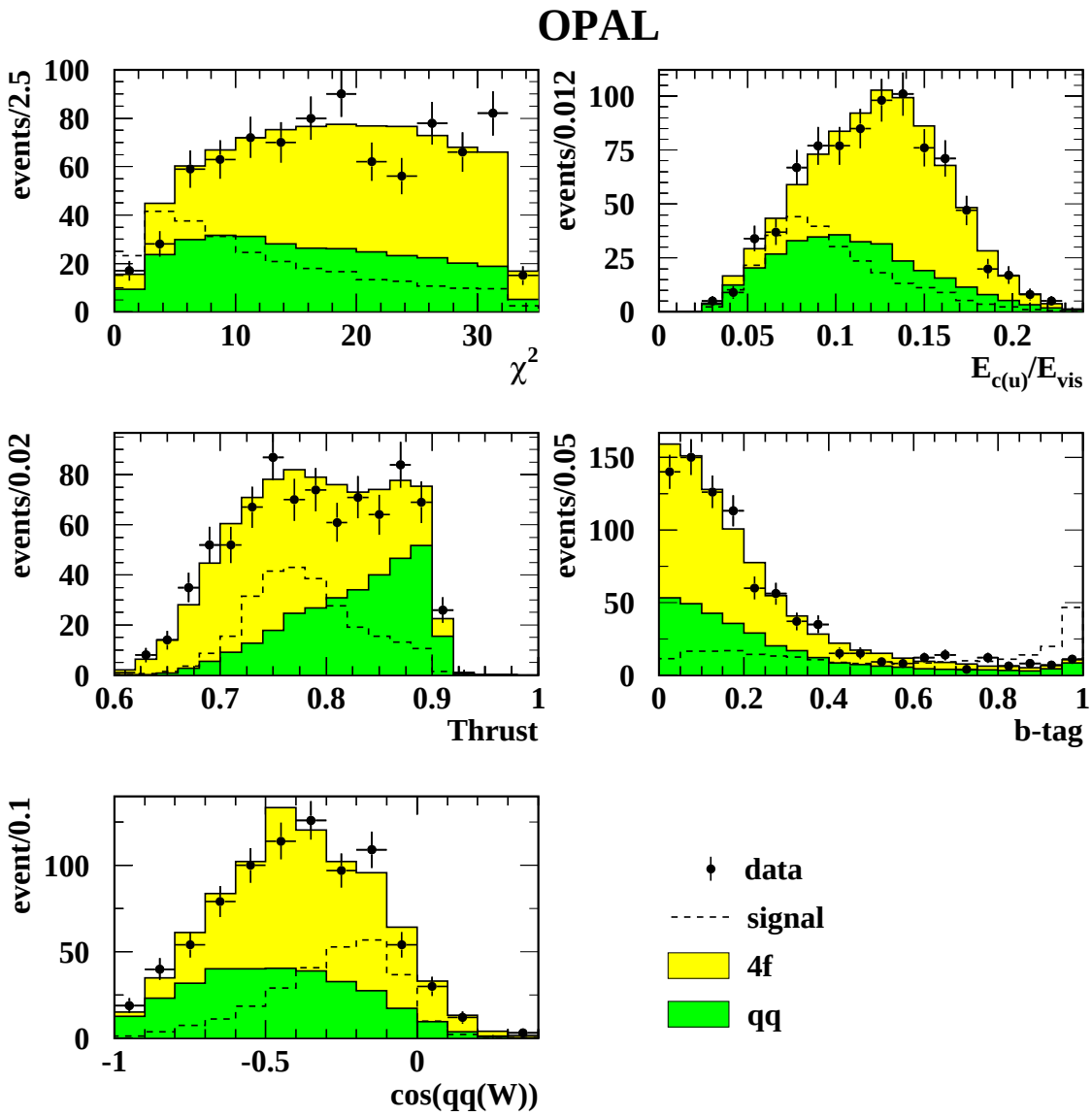

Figure 2: Distributions of the likelihood variables for the hadronic channel at $\sqrt{s} \simeq 189\,\mathrm{GeV}$. Comparisons between the data, the SM 4-fermion (light grey), and $\mathrm{q\bar{q}}$ backgrounds (grey) are shown. The dashed line represents single top MC events with $m_{\mathrm{t}} = 174\,\mathrm{GeV/c^2}$ and an arbitrary cross-section of $\sigma_{\mathrm{top}} = 3\,\mathrm{pb}$.

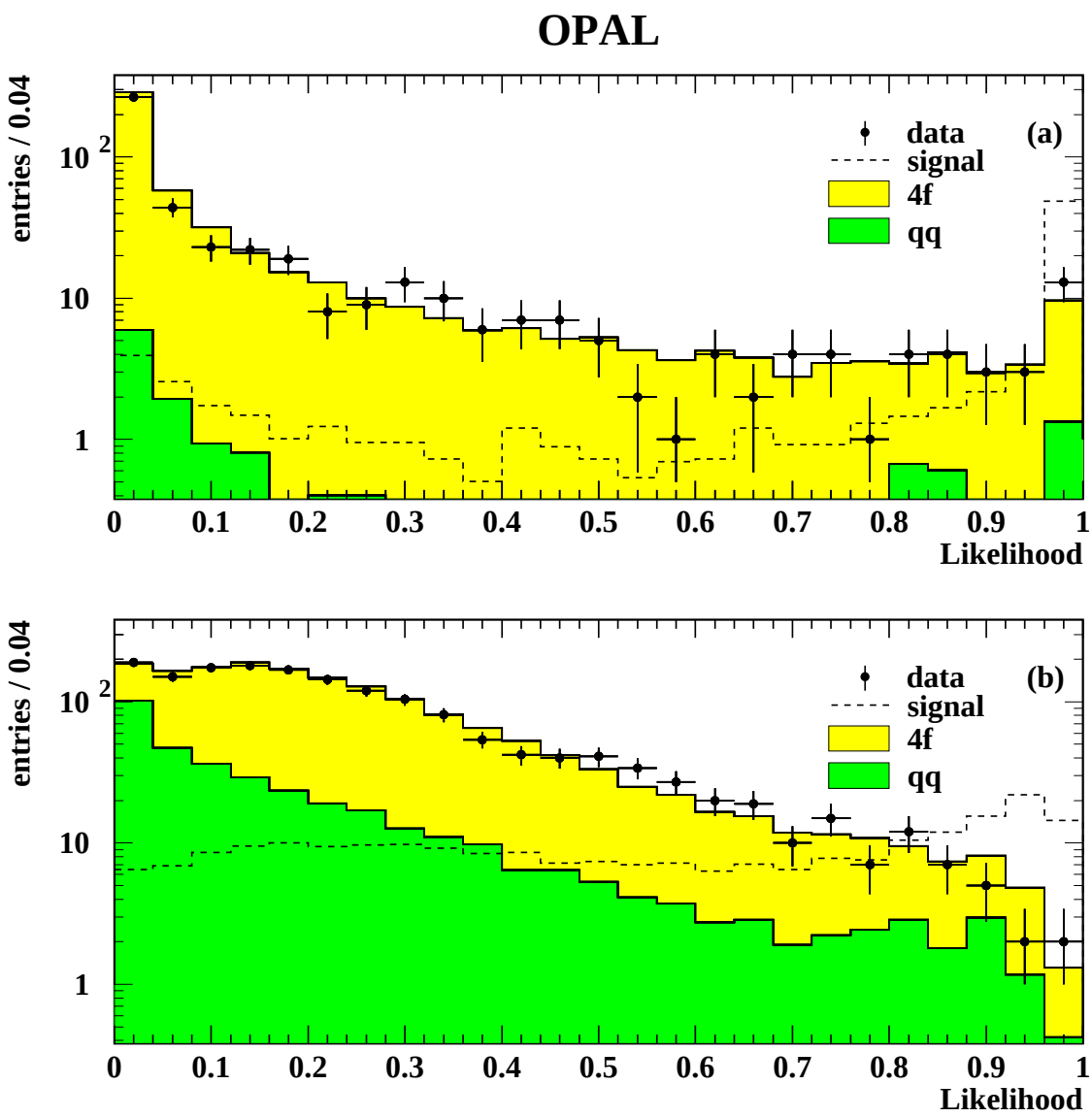

Figure 3: Distributions of the likelihood variables for (a) the leptonic and (b) the hadronic channels. The comparison between the data collected in 2000 at $\sqrt{s} \simeq 205\,\mathrm{GeV}$ and $\sqrt{s} \simeq 207\,\mathrm{GeV}$, the SM 4-fermion (light grey), and the $\mathrm{q\bar{q}}$ backgrounds (grey) is shown. The dashed line represents single top MC events with $m_{\mathrm{t}} = 174\,\mathrm{GeV/c^2}$ and an arbitrary cross-section of $\sigma_{\mathrm{top}} = 3\,\mathrm{pb}$.

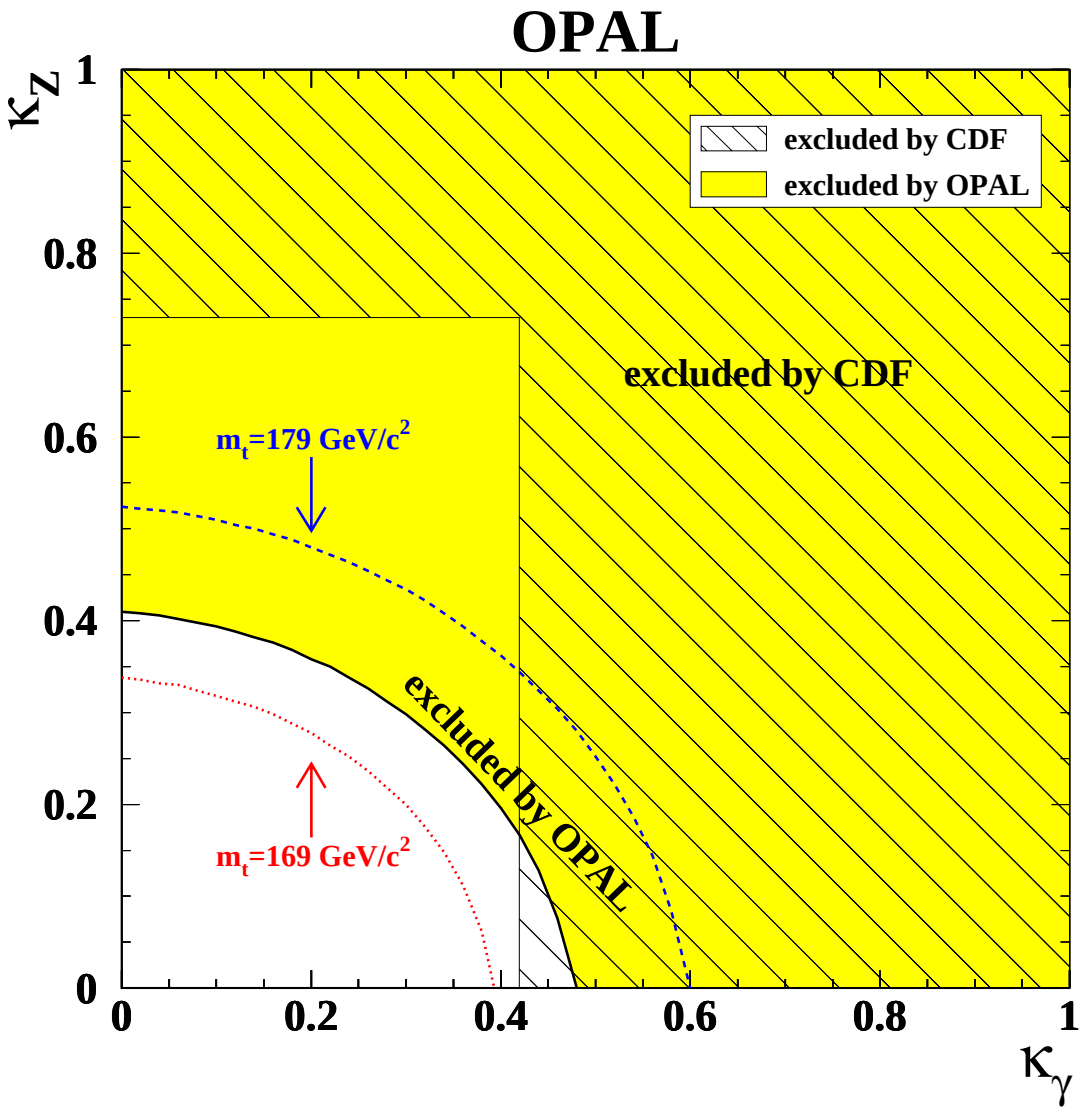

Figure 4: The light grey region shows the OPAL exclusion region at 95% CL in the $\kappa_Z - \kappa_\gamma$ plane for $m_t = 174\,\mathrm{GeV}/c^2$. The exclusion curves for different values of top quark masses are also shown. The hatched area shows the CDF exclusion region [9]. The OPAL limits include QCD and ISR corrections to the Born-level cross-section defined in Equation 2.